Research Paper

Mitochondria-Responsive Drug Release along with Heat Shock Mediated by Multifunctional Glycolipid Micelles for Precise Cancer Chemo-Phototherapy

Yanan Tan[2], Yun Zhu[2], Lijuan Wen[1], Xiqin Yang[1], Xuan Liu[1], Tingting Meng[1], Suhuan Dai[1], Yuan Ping[1], Hong Yuan[1], and Fuqiang Hu[1,2✉]

1. College of Pharmaceutical Science, Zhejiang University, 866 Yuhangtang Road, Hangzhou 310058, China
2. Ocean College, Zhejiang University, 1 Zheda Road, Zhoushan 316021, China

✉ Corresponding author: Prof. Fuqiang Hu, Tel/Fax: +86-571-88208439, E-mail: hufq@zju.edu.cn

Abstract

Responsive drug release in tumor mitochondria is a pre-requisite for mitochondria-targeted drug delivery systems to improve the efficacy of this promising therapeutic modality. To this end, a photothermal stimulation strategy for mitochondria-responsive drug release along with heat shock is developed to maximize the antitumor effects with minimal side effects.

Methods: This strategy relies on mitochondrial-targeted delivery of doxorubicin (DOX) through a photothermal and lipophilic agent IR-780 iodide (IR780)-modified glycolipid conjugates (CSOSA), which can synergistically triggers high-level reactive oxygen species (ROS) to kill tumor cells.

Results: Specifically, upon laser irradiation, the photothermal conversion by IR780-CSOSA can not only weaken the hydrophobic interaction between the core of micelles and DOX and trigger unexpected micelle swelling to release DOX in mitochondria for the amplification of ROS, but also induce mitochondria-specific heat shock to promote the fast evolution of ROS at the same locus to eradicate cancer cells in a more effective way. Furthermore, IR780-CSOSA micelles may independently realize the real-time diagnosis and imaging on multiple tumor models. Deep penetration into tumors by IR780-CSOSA/DOX micelles can be manipulated under laser irradiation.

Conclusion: Such multifunctional IR780-CSOSA/DOX micelles with integration of mitochondria-responsive drug release and heat shock are demonstrated to be superior to the non-mitochondria-responsive therapy. This study opens up new avenues for the future cancer diagnosis and treatment.

Key words: mitochondria-responsive drug release, mitochondrial heat shock, glycolipid micelles, photothermal therapy, chemotherapy

Introduction

Nanotechnology has the potential to make a significant impact in cancer therapy by various approaches including an enhanced toxicity profile of the loaded chemotherapeutic drugs [1]. Since many drugs act on intracellular sites within specific subcellular organelles [2], functionalization of nanocarriers for organelle-specific delivery of bioactive molecules to specific intracellular compartments can sharply enhance the efficiency of various treatment protocols and reduce incidence of adverse effects [3]. Consequently, efficient targeting and responsive drug release in subcellular organelle is a pre-requisite for nanocarriers.

Mitochondrion is a key subcellular organelle, which mainly regulates the intrinsic apoptosis pathway and can be regarded as the major target for initiating tumor cell apoptosis by disrupting the balance of mitochondrial ROS in cancer treatment

[4-6]. Although many studies on mitochondria-targeted nanoparticles (based on mitochondriotropic lipophilic cations [7, 8] or mitochondria-penetrating peptides [9, 10]) for cancer treatment have been reported, the leakage of drug in cytoplasm and lysosome are common issues once the therapeutic nanoparticles are transported inside the tumor cells [11, 12]. Only with the sufficient drug concentration in tumor mitochondria can drug delivery systems (DDSs) contribute to better therapeutic effects [13-16]. Therefore, responsive drug release inside mitochondria is urgently essential [17, 18].

The mitochondrial microenvironments as well as the external stimulation are potential triggers for designing mitochondria-responsive DDSs. Although the high-level glutathione (GSH) or ROS in tumor mitochondria matrix [19, 20], can be leveraged to improve the drug release at target sites, these pathological signals are likewise to present throughout cytoplasm without significant gradient distribution. The internal pathological signal that can trigger drug release inside tumor mitochondria is limited. Consequently, the development of external triggers, such as light or heat, may become alternative options to enhance drug release at mitochondria. Significantly, the local hyperthermia generated by photothermal agents under NIR laser irradiation could be taken advantage of to weaken the interaction relationship between the drug and nanocarrier, facilitating fast release of drug loaded in nanocarriers. Indeed, by incorporation of the specific photothermal material into a drug delivery carrier, one can speculate that mitochondrial targeting and drug release mediated by such nanocarriers could be largely improved, owing to the synergistical effect of energy-dependent cell uptake and transport into mitochondria as well as the photothermal-induced drug release. Such a DDS clearly distinguish from the conventional mitochondria-targeted ones in terms of their controllability and sensitivity.

As well documented, tumor mitochondria are hypersensitive to heat shock [21-26], ultimately inducing cell apoptosis by elevating the generation of ROS [27]. In addition, the previous report on the magnetic nanoparticle modified with a mitochondria-targeting peptide for cancer photothermal therapy (PTT) has demonstrated that mitochondria are also readily sensitive to hyperthermia [28]. Taking these advantages, we hypothesize that a NIR-responsive DDS with chemotherapeutic and photothermal capabilities can maximize the synergistic antitumor effects of chemotherapy and PTT with minimal side effects, by means of mitochondria-responsive drug release and heat shock. The local cytotoxic drug accumulation and heat shock can jointly induce the localized ROS burst in tumor mitochondria, leading to the activation of mitochondria-mediated intrinsic apoptosis pathway [29, 30]. Compared with those existing combined chemotherapy and PTT [31-36], the DDS with mitochondria-responsive drug release and heat shock capabilities for precise cancer chemo-phototherapy is exhilarating, which has been rarely reported.

In order to achieve local responsive drug release and hyperthermal effect in mitochondria, a critical challenge is to design the appropriate delivery carriers that can transport both photothermal agents and chemotherapeutic drugs to fully overcome a series of physiological barriers at both extracellular and intracellular levels. Chitosan is an ideal natural biodegradable polycation biomacromolecule and positively charged chitosan groups with proton buffering ability can achieve better endosomal/ lysosomal escape via the proton sponge effect [37], providing a huge potential in developing mitochondria-targeted DDSs.

In this study, we aim to construct a NIR-triggered DDS that can induce mitochondria-responsive drug release and achieve mitochondria-specific heat shock for the precise and effective combination therapy. We chose IR780 (IR-780 iodide), a NIR-responsive lipophilic photothermal agent [38] with preferential tumor mitochondria-specific accumulation capability through both the organic-anion-transporting polypeptide (OATP)-mediated active transport and the lipophilic cation characters for *in vivo* imaging [39-43], to modify glycolipid-like conjugates (CSOSA). The resulted amphiphilic polymer, termed as IR780-CSOSA, can self-assemble into micelles above its critical micelle concentration (CMC). The doxorubicin (DOX)-loaded IR780-CSOSA (IR780-CSOSA/DOX) micelles are capable of targeting tumor mitochondria, thereby triggering photothermal conversion and local drug release upon NIR-laser irradiation. On one hand, the resulted hyperthermia at mitochondria enhances DOX solubility and reduces hydrophobic interaction between hydrophobic core of micelles and DOX, leading to mitochondrial fast drug release for amplifying ROS evolution. On the other hand, the photothermal conversion also induces mitochondrial heat shock effect to enhance ROS evolution to kill cancer cells. These two effects can jointly induce cancer cell apoptosis to inhibit tumor growth (**Figure 1**).

Materials and methods

Materials

IR-780 iodide (IR780) was provided by Life Technologies (Carlsbad, CA, USA). Aladdin Reagent

Co., Ltd. (Shanghai, China) supplied TEA and pyrene. Shanghai Medpep Co, Ltd provided 1-ethyl-3-(3-dimethyl-aminopropyl) carbodiimide (EDC). Chitosan (CSO, Mw 19 kDa) was acquired with enzymatic degradation of chitosan (95% deacetylated, 450 kDa, purchased from Yuhuan Marine Biochemistry Co., Ltd, Zhejiang, China). Shanghai Chemical Reagent Co., Ltd provided stearic acid (SA). Flourescein isothiocyanate (FITC), 2,4,6-trinitrobenzenesulfonic acid (TNBS) and methylthiazoletetrazolium (MTT) were supplied by Sigma Chemical Co. Meilun Biology Technology (Dalian, China) provided doxorubicin hydrochlorate (DOX·HCl). Dyadic International Inc. (Jupiter, Florida) provided chitosanase. Beyotime Biotechnology, Co., Ltd (Beijing, China) offered strep-tavidin-peroxidase immunohistochemical kit and dichlorodihydrofluorescein diacetate (H2DCFDA). Gibco (Merelbeke, Belgium) offered Dulbecco's modified Eagle's medium (DMEM) and trypsin. Sijiqing Biology Engineering Materials Co, Ltd (Zhejiang, China) provided fetal bovine serum.
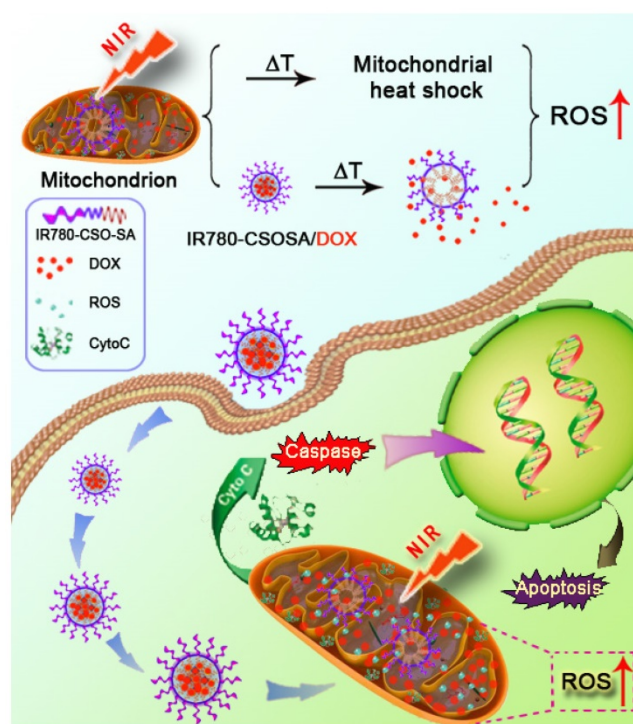

Figure 1. The NIR-triggered drug delivery system with mitochondria-responsive drug release and heat shock capabilities. IR780-CSOSA/DOX micelles selectively targeted into tumor mitochondria and realized photothermal conversion upon NIR-laser irradiation, which photothermally triggered drug release and heat shock in mitochondria, resulting in domino effect on ROS burst for cell apoptosis to perform maximized antitumor efficacy.

Synthesis of IR780-CSOSA

Firstly, we prepared the glycolipid-like polymer CSOSA as the method reported previously. In brief, EDC and SA were dissolved in ethanol, and then stirred at 60 °C for 45 min. CSO was dissolved in deionized (DI) water at 60 °C for 10 min. Afterwards, the mixture of SA and EDC was added dropwise into the aqueous solution and stirred at 60 °C. After another 12 h, the reaction solution was poured into a dialysis bag (MWCO: 7 kDa) for 96 h dialysis with DI water. The product CSOSA was acquired with lyophilizing and washing in hot ethanol to get rid of byproducts.

For the synthesis of IR780 modified CSOSA, TEA was applied as an acid-binding agent. IR780 (10 mg) was dissolved DMSO (7 mL), and TEA with the mol ratio 2:1 was added, then stirred at 60 °C for 12 h. After that, CSOSA (12.1 mg) was dissolved in DI water (2 mL) and the previous mixture was dropwise added and stirred at 60 °C for another day. The reaction solution was dialyzed in DI water for three days and further centrifuged for 10 min at 8000 rpm to remove the by-product. The supernatant was collected and then lyophilized as the final reaction product.

Preparation of DOX-loaded micelles

The model drug doxorubicin base (DOX) was obtained according to the previous study. The DOX-loaded micelles were acquired with dialysis method. In brief, 2 mg/mL of DOX/DMSO was dropwise added into 2 mg/mL of IR780-CSOSA or CSOSA aqueous solution and stirred for 2 h. Then, we dialyzed the mixture solution in DI water overnight and centrifugated for 10 min at 8000 rpm to get rid of the unencapsulated DOX. The supernatant was collected as the IR780-CSOSA/DOX or CSOSA/DOX micelles. Afterwards, a HPLC system was used to detect the amount of encapsulated DOX in micelles. The mobile phase was comprised of methanol-acetonitrile-0.01 mol/L SDS containing 0.6‰ phosphoric acid (60:30:10, v/v, 1.0 mL/min) at 25 °C. Ultraviolet absorption wavelength was 254 nm. Drug loading (DL%) and drug encapsulation efficiency (EE%) of DOX-loaded micelles were calculated as following formulas.

$$DL\% = \frac{\text{Weight of DOX in micelles}}{\text{Weight of DOX-loaded micelles}} \times 100\% \quad \text{Equation (1)}$$

$$EE\% = \frac{\text{Weight of DOX in micelles}}{\text{Weight of DOX in feed}} \times 100\% \quad \text{Equation (2)}$$

Characteristics of IR780-CSOSA and DOX-loaded micelles

For the verification on chemical structure of IR780-CSOSA conjugate, we applied a ^{1}H NMR spectrometer (AC-80, Bruker Biospin, Germany) to determine the ^{1}H NMR spectra of IR780, CSOSA and IR780-CSOSA conjugate, respectively. The spectrum of IR780-CSOSA was verified by UV-vis spectra (UV-1800, Persee General Instrument Ltd, Beijing). TNBS test was applied to detect the amino

substitution degree (SD %) on micelles. As IR780 had a strong absorption at 795 nm, the ratio of IR780 on CSOSA was measured by UV-vis spectra of both IR780 solution and IR780-CSOSA micelles. A temperature probe was inserted to monitor the temperature elevation of each sample. IR780 solution (10 μg/mL, 1 μg/mL) and IR780-CSOSA micelles (equivalent IR780: 10 μg/mL, 1 μg/mL) were respectively exposed to an 808 nm NIR-laser (1 W/cm^2) for 5 min. Equal volume of PBS was used as control. To further evaluate the photothermal stability of IR780-CSOSA micelles, five cycles of irradiations were performed and each cycle of irradiation lasted 4 min (808 nm, 1 W/cm^2). The sample temperature was measured. The UV-vis absorbance was also recorded after repeated irradiations including free IR780 and IR780-CSOSA micelles. CMC of micelles was detected using pyrene probe. We used a Zetasizer (3000HS, Malvern Instruments Ltd, UK) to determine the sizes and zeta potentials of blank and DOX-loaded micelles (1 mg/mL in DI water). Also, the size changes of IR780-CSOSA/DOX micelles in PBS, saline and DMEM during 48 h were determined by a Zetasizer.

NIR-triggered drug release *in vitro*

Drug release profile of DOX-loaded micelles was studied by dialyzing in pH 6.8 PBS in an incubator shaker with horizontal shaking (75 rpm) at 37 °C. 1.0 mL of IR780-CSOSA/DOX or CSOSA/DOX solution was dialyzed against 20.0 mL PBS (MWCO: 3.5 kDa). To investigate NIR-triggered DOX release, IR780-CSOSA/DOX and CSOSA/DOX solution after incubated in pH 6.8 PBS for 4 h were exposed to a laser (808 nm, 1 W/cm^2) for 3 min. At appointed time points, all of medium outside of dialysis bag was obtained and replaced by fresh PBS. DOX concentration of all the samples before and after NIR-laser irradiation was determined with a fluorescence spectrophotometer, and the assays were repeated three times.

NIR-triggered destabilization of IR780-CSOSA/DOX

Size changes of IR780-CSOSA and IR780-CSOSA/DOX micelles were detected by DLS in various temperature (4 °C, 25 °C, 37 °C, 43 °C, 56 °C). The morphology changes of the micelles in 37 °C and 56 °C were observed by a TEM (JEOL, JEM-1230, Japan). Blank CSOSA and CSOSA/DOX micelles were as control groups. The solubility of DOX in pH 6.8 PBS at different temperature (37 °C,43 °C,56 °C) was measured by incubating excess DOX in an incubator shaker with horizontal shaking (75 rpm), respectively. After 48 h, we collected the supernatant to measure the DOX concentration with a fluorescence spectrophotometer, and the assays were repeated three times.

Cell culture

Human breast adenocarcinoma cells (MCF-7) or human hepatocellular carcinoma cells (HepG2) or mouse breast adenocarcinoma cells (4T1) or mouse hepatocarcinoma cells (H22) were cultured in DMEM containing 10% fetal bovine serum at 37 °C in a humidified atmosphere with 5% CO$_2$.

In vitro co-localization of micelles into mitochondria

To investigate the cellular uptake, we prepared FITC-labeled IR780-CSOSA or CSOSA micelles as previous work. In brief, added dropwise FITC ethanol solution (2.0 mg/mL) into 2.0 mg/mL IR780-CSOSA or CSOSA aqueous solution (micelles: FITC = 1:1, mol: mol), further stirred for 4 h in aphotic environment and dialyzed against DI water overnight to get rid of redundant FITC and ethanol. We finally obtained FITC labeled micelles (FITC-IR780-CSOSA or FITC-CSOSA) solution. To analyze the cellular uptake quantitatively, MCF-7 or HepG2 cells were exposed to FITC labeled micelles for 1, 4 and 12 h, then washed and resuspended by PBS. A flow cytometry (FACS) (FC 500 MCL; Beckman Coulter, USA) was used to determine the intensity of cellular fluorescence.

To confirm the mitochondrial co-localization of micelles with or without laser irradiation *in vitro*, we observed the cellular internalization of IR780-CSOSA or CSOSA micelles using by a confocal laser scanning microscope (CLSM) (Ix81-FV1000, Olympus, Co.,). In brief, we seeded 2×10^4 MCF-7 cells per well into 24-well plates containing sterilized coverslips. After incubation at 37 °C for 24 h, the cells were respectively cultured with the same molar weight of FITC-IR780-CSOSA or FITC-CSOSA for 4 h and the ratio of FITC and IR780-CSOSA or CSOSA was 1:1. Then, the cells were treated with a laser for 3 min (808 nm, 1 W/cm^2) and continuously incubated for 2, 4 h and 8 h. The cell mitochondria were stained with 100 nM of MitoTracker Red FM solutions at 37 °C for 30 min. After washed in PBS three times, the cells were viewed with a CLSM. After that, the MFI of micelles and the co-localization coefficient were calculated by ImageJ software.

NIR-triggered drug release inside mitochondria

2×10^4 cells/well MCF-7 cells were placed in 24-well plates containing coverslips and cultured overnight. Subsequently, cells were exposed to CSOSA/DOX or IR780-CSOSA/DOX (equivalent DOX: 1.5 μg/mL) and kept in an incubator for 4 h. Next, the culture medium were displaced by fresh medium to remove uninternalized nanoparticles and irradiated with or without laser for 3 min (808 nm, 1

W/cm^2), then continuously incubated for 4 h and 8 h. The cell mitochondria were stained with 100 nM of MitoTracker Green FM solutions at 37 °C for 30 min. After washed in PBS three times, all the cell samples were fixed and visualized by a CLSM. After that, we used an ImageJ software to calculate the MFI of DOX and co-localization coefficient of released DOX and mitochondria.

Cytotoxicity

MTT assays were applied to determine the cytotoxicity of DOX-loaded micelles under laser irradiation. In brief, 4×10^3 cells /well MCF-7 cells were placed in 96-well culture plates. After culturing at 37 °C for 24 h, the cells were exposed to various formulations for 4 h, including different DOX concentrations of IR780-CSOSA, DOX, CSOSA/DOX and IR780-CSOSA/DOX, and then irradiated with or without laser for 3 min (808 nm, 1 W/cm^2). After re-incubation for additional 44 h, cells in each well were added with 20.0 µL of MTT solution (5.0 mg/mL) and further cultured at 37 °C for 4 h. The medium was replaced by 200 µL of DMSO to dissolve purple formazan crystals. We applied a microplate reader (Bio-Rad, Model 680, USA) to detect the absorbance of each well at 570 nm. The assays were repeated three times.

Mitochondrial apoptosis signaling pathways

The measurement of ROS levels

H_2DCFDA was applied for determining the production of intracellular ROS, which was quantified by increased fluorescence intensity using a FACS. Briefly, MCF-7 cells were exposed to blank, free DOX, IR780-CSOSA, CSOSA/DOX and IR780-CSOSA/ DOX micelles (equivalent DOX: 2 µg/mL, equivalent IR780: 0.5 µg/mL) for 4 h. Thereafter, cells treated with formulations were exposed to a laser for 3 min (808 nm, 1 W/cm^2) and continuously cultured. After another 12 h, cells were treated with H_2DCFDA stock solution (10 µM) and incubated for 30 min in aphotic environment. Finally, cells were washed and resuspended by PBS, and a FACS was used to measure the fluorescence intensity immediately. Meanwhile, MCF-7 cells exposed to various formulations without laser irradiation were evaluated in a similar manner.

Western blot

1×10^6 cells/well MCF-7 cells were placed into 6-well plates and incubated overnight. The cells were cultured with blank, DOX, CSOSA/DOX, IR780-CSOSA and IR780-CSOSA/DOX micelles (equivalent DOX: 2 µg/mL, equivalent IR780: 0.5 µg/mL) for 4 h incubation. Subsequently, they were treated with a laser for 3 min (808 nm, 1 W/cm^2). After incubated for another 20 h, cells were washed by PBS and lysed by a buffer with protease inhibitors and Triton X-100. We used sodium dodecyl sulfate-polyacrylamide gel electrophoresis to recover and separate proteins, which were subsequently shifted to a PVDF membrane and blocked using 5% fat-free milk. Subsequently, the diluted primary antibodies were incubated at 4 °C for 12 h, including cytochrome c (1/1000, servicebio), cleaved caspase-3 (1/1000, CST), cleaved caspase-9 (1/1000, CST) and actin (1/1000, Mouse, Sigma), then incubated with secondary antibody. Finally, ECL reagent was used to detect the proteins according to the protocols. The expression of heat shock protein 70 (HSP70) was determined on MCF-7 cells exposed to IR780-CSOSA/DOX with laser for 0, 1, 2 and 3 min (808 nm, 1 W/cm^2), respectively. Meanwhile, MCF-7 cells treated with PBS with or without laser for 3 min (808 nm, 1 W/cm^2) were as control groups and evaluated in a similar manner.

In vivo imaging

For the preparation of three different tumor-bearing mice models, all the animal studies were carried out in accordance with the guidelines authorized via Ethical Committee of Zhejiang University. 100 µL of MCF-7 cells suspension (1×10^7 cells in PBS) was inoculated subcutaneously at the blank of nude mice (female, 6-8 weeks). 4T1 tumors on the right mammary gland of BALB/c mice (female) were initiated with injection of 100 µL of 4T1 cells suspension (1×10^5 cells in PBS). H22 tumors were subcutaneously inoculated in the BALB/c mice with injection of 100 µL of H22 cells suspension (2×10^6 cells in PBS). When tumor size of three tumor models reached to the requirement, IR780-CSOSA (equivalent IR780: 0.5 mg/kg) was injected intravenously to confirm the tumor targeting efficacy and imaging potential, respectively. At the appointed time, tumor-xenografted mice models were imaged via a Maestro *in vivo* Imaging System (CRI Inc.,).

Temperature measurement under NIR-laser irradiation *in vivo*

The MCF-7 tumor-xenografted mice were respectively injected *via* the tail vein with saline, CSOSA/DOX and IR780-CSOSA/DOX (200 µL, equivalent DOX: 2 mg/kg) to investigate intratumoral temperature changes under laser irradiation. The tumors were exposed to a laser for 5 min (808 nm, 0.5 W/cm^2). We used the infrared thermal imaging camera to record the infrared thermographic maps and region maximum temperatures.

The penetration study *in vitro* and *in vivo*

A 96-well plate (Corning, USA) was firstly covered with autoclaved agarose solution (1.5%, w/v) at 50 µL/well and then cooled to room temperature. Mixed NIH 3T3 and MCF-7cells (1:1, 2 × 10³ cells/well) were seeded and cultured for 4 days to grow into multi-cellular tumor spheroid model (MCTS), simulating the structure of solid tumor. The formation of MCTS was monitored using optical microscope (TE2000-S, Nikon, Japan). The tumor spheroids were exposed to IR780-CSOSA/DOX or CSOSA/DOX (equivalent DOX: 1.5 µg/mL) for 4 h. Subsequently, tumor spheroids were respectively treated with or without laser for 3 min (808 nm, 1 W/cm²) and continuously cultured for 20 h. Subsequently, tumor spheroids were washed by PBS, fixed and placed in cavity microscope slides. The CLSM images were obtained using Z-stack Tomoscan with 5 µm intervals from the top to the middle of the spheroid.

To investigate the penetration ability *in vivo*, the IR780-CSOSA/DOX and CSOSA/DOX micelles (200 µL, equivalent DOX: 2 mg/kg) were intravenously injected. After one day, tumors on MCF-7 tumor-xenografted mice were treated with or without laser irradiation for 3 min (808nm, 0.5 W/cm²). After another day, the mice were euthanized and tumors were obtained. Next, tumors were embedded with OCT and then frozen in liquid N_2. Finally, tumors were sectioned and stained with DAPI, then analyzed by the CLSM.

In vivo chemo-photothermal therapy efficiency

All the tumor-xenografted mice models were randomly seperated into ten groups (n = 6), as follows: saline, DOX·HCl, CSOSA/DOX, IR780-CSOSA and IR780-CSOSA/DOX (equivalent DOX: 2 mg/kg, equivalent IR780: 0.5 mg/kg) with or without laser, respectively. Ten formulations were injected every two days during first 9 days after the tumor volume reach about 200 mm³. For laser treatment groups, the tumors were exposed to a laser for 3 min (808 nm, 0.5 W/cm²) on the day after injection. To evaluate the antitumor efficiency and safety, tumor volumes and mice weights were recorded every other day post administration in 21 days. Survival times of these mice are recorded in 40 days. The mice were all euthanized. The tumors and other organs in various groups were fixed and sliced for HE staining. To further verify the mechanism of synergistic antitumor efficiency, the tumor samples were sliced and analyzed by immunohistochemistry assessments on HSP70, cleaved caspase-3, Ki67, CD 31 and immunofluorescence assessment on CD 8 levels.

Statistical analysis

The results were presented as the mean ± standard deviation of three separate experiments. We applied student's t-test to examine significant differences between groups and $p<0.05$ were regarded significant statistically.

Results and discussion

Preparation and characteristics of IR780-CSOSA

To synthesize IR780-CSOSA, the glycolipid cation polymer CSOSA was first obtained by coupling reactions between carboxyl groups of SA and amino groups of CSO using dehydrating agent EDC [44]. Subsequently, IR780-CSOSA was acquired with substitution reactions between chlorine atom of IR780 and amino groups of CSOSA using an acid-binding agent triethylamine (TEA) (**Figure 2**A). ¹H NMR spectrum was used to confirm the chemical structure of IR780-CSOSA (Figure 2B). From the spectrum of IR780-CSOSA, the peaks at 3.76, 2.74 and 1.91 ppm were from the proton of -CH_2O-, -CHN- and -NH_2 on CSOSA, respectively. Characteristic peaks at 7.40 ppm (magnified portion in Figure 2B) was attributed to the proton from benzene ring on IR780. The above results illustrated that IR780 was successfully conjugated onto CSOSA. After IR780 modification, IR780-CSOSA micelles still exhibited the strong absorption at 795 nm (Figure 2C), thereby well reserving the photothermal potential of native IR780. The SD % of CSOSA was 16.81% measured using TNBS test [45]. The molar ratio of IR780 on IR780-CSOSA measured by UV-vis spectra was calculated as 3.12%. The CMC values of IR780-CSOSA and CSOSA were respectively determined as 62.4 µg/mL and 29.2 µg/mL with a fluorescent probe pyrene [46]. The size of IR780-CSOSA was 149.7 ± 2.5 nm, which was larger than that of CSOSA (85.0 ± 3.8 nm) (**Table S1**). Furthermore, the zeta potential of IR780-CSOSA was 39.4 ± 0.6 mV and marginally higher than that of CSOSA (37.4±1.5 mV). The increased size and zeta potential were probably due to lipophilic cation IR780 modified on the surface of CSOSA. However, after loading drug, the size of IR780-CSOSA/DOX and CSOSA/DOX respectively decreased to 119.0 ± 7.6 nm and 48.4 ± 1.1 nm (Table S2). The decreased size could be owing to the increased hydrophobic interaction between DOX and micellar core, which made the micellar core more compact and stable [47]. To evaluate the stability of micelles *in vitro*, we determined the size changes of IR780-CSOSA/DOX micelles during 48 h incubation within PBS, saline and DMEM. As shown in **Figure S1**, the sizes of IR780-CSOSA/DOX micelles in PBS, saline and

DMEM were constantly maintained about 120 nm for 48 h, indicating the preferable stability of IR780-CSOSA/DOX micelles. DOX was loaded commendably in IR780-CSOSA micelles with the EE% of 81.1% and DL% of 10.9%, respectively (Table S2).

IR780 (10 µg/mL) achieved the certain photothermal property as the temperature increased by 26.3 °C after irradiated with a laser for 5 min (808 nm, 1 W/cm2) (Figure 2D). By contrast, a pronounced increase of temperature from 26.4 °C to 55.8 °C was observed for the suspension of IR780-CSOSA (equivalent IR780: 10 µg/mL) micelles. When the concentration of IR780 was 1 µg/mL, IR780 or IR780-CSOSA exhibited similar temperature elevating ability. These results indicated the modification on the micelles had no influence on the photothermal conversion ability of IR780. Additionally, the photothermal conversion efficiency (η) of IR780-CSOSA was calculated to be 33.5%. (Supplementary Information and Figure S2 for the detailed

calculations) To further evaluate the photothermal stability of IR780-CSOSA micelles under repeated irradiation, we determined the UV-vis absorbance curves and photothermal curves of free IR780 and IR780-CSOSA micelles during five cycles of irradiations (Figure S3). After the first cycle of irradiation, free IR780 exhibited 91.5% decrease of absorbance at 795 nm, indicating free IR780 was rapidly degraded after laser irradiation. Conversely, IR780-CSOSA micelles showed only 13.1% decrease of absorbance at 795 nm during the same period and obtained over 90% decrease of absorbance until 3 cycles of irradiation, illustrating IR780-CSOSA micelles could protect IR780 from degradation after laser irradiation. Consequently, the temperature increase produced by IR780-CSOSA micelles was significantly higher than those produced by free IR780 after repeated irradiation, indicating effective photothermal conversion ability of IR780-CSOSA micelles.
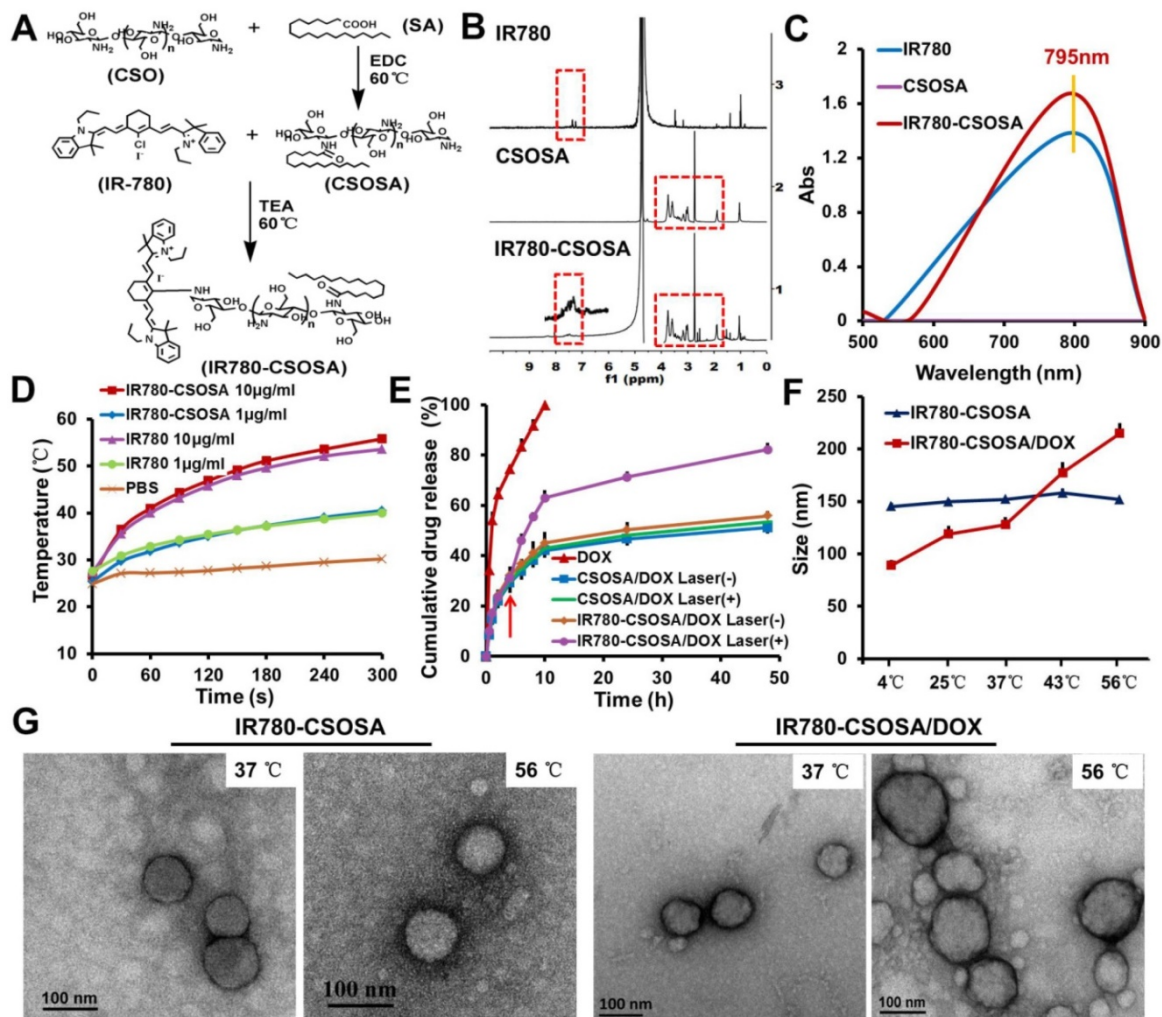

Figure 2. Characterization of IR780-CSOSA micelles. (A) Synthetic route of IR780-CSOSA. (B) 1H NMR spectra of IR780, CSOSA and IR780-CSOSA. The characteristic peaks are pointed out and magnified (upper). (C) UV-vis spectra of IR780, CSOSA and IR780-CSOSA solution. (D) Photothermal effect of IR780-CSOSA and free IR780 under laser irradiation (808nm, 1W/cm2) for 5 min. (E) *In vitro* NIR-triggered drug release profiles. IR780-CSOSA/DOX and CSOSA/DOX solutions after incubated in pH 6.8 PBS for 4 h were irradiated with or without laser (808 nm, 1 W/cm2) for 3 min. (n = 3). (F) Size changes of IR780-CSOSA and IR780-CSOSA/DOX micelles at different temperatures by Zetasizer. (G) Transmission electron microscope (TEM) images of IR780-CSOSA and IR780-CSOSA/DOX micelles at 37 °C and 56 °C.

In vitro measurement on NIR-triggered drug release

As expected above, IR780-CSOSA micelles exhibited a pronounced photothermal property. To investigate whether the hyperthermia induced by NIR-laser irradiation could trigger efficient drug release, we measured drug release behavior of micelles at different time points (Figure 2E). Both IR780-CSOSA/DOX and CSOSA/DOX micelles exhibited slow drug release during the first 4 hours. However, when IR780-CSOSA/DOX micelle solution was irradiated with a laser (808nm, 1 W/cm^2, 3 min) after 4 h incubation, a fast release behavior was observed in the first 10 h with a total release rate of 62.95%. As expected, the total release rate of DOX increased to 82.25% up to a release period of 48 h. Under the same condition, however, CSOSA/DOX micelles continuously exhibited a slow drug release behavior during the whole release window, with a total release rate of 53.48% at 48 h. These results suggested that IR780-CSOSA/DOX could realize fast drug release in response to NIR-laser irradiation, probably due to the enhanced water solubility of DOX and reduced hydrophobic interaction under hyperthermal condition. To further confirm our hypothesis, the size changes of blank and DOX-loaded micelles at various temperature (4 °C, 25 °C, 37 °C, 43 °C, 56 °C) were determined by DLS (Figure 2F). The size of IR780-CSOSA/DOX micelles increased with the temperature elevating and reached 215.0 ± 9.6 nm at 56 °C, which is significantly larger than that at 37 °C (123.0 ± 7.0 nm). In addition, TEM images, where IR780-CSOSA/DOX micelles showed larger size at 56 °C over 37 °C, further validate our postulation (Figure 2G). Also, CSOSA/DOX micelles exhibited the similar size increase at high temperature (Figure S4 and S5). By contrast, the size of blank micelles (without DOX loading) kept stable with the increase of temperature. The solubility of DOX at pH 6.8 were determined as 19.50 ± 0.18 μg/mL at 56 °C, which was 2.75 times that at 37 °C (Table S3). These results implied that the enhanced water solubility of DOX at the hyperthermal condition contributed to the fast drug release [48, 49], as a consequence of reduced hydrophobic interaction between hydrophobic core of micelles and DOX [50-52]. The above also explained why the micelles are more prone to swell at high temperature. Collectively, by taking advantage of the photothermal ability of IR780-CSOSA micelles to induce local hyperthermia, we are able to control the drug release kinetics successfully [53, 54].

Cellular internalization and mitochondrial co-localization of micelles

We subsequently analyzed the cellular uptake of IR780-CSOSA micelles with flow cytometry. As shown in Figure S6 and S7, IR780-CSOSA micelles have noticeably enhanced intensity of green fluorescence on MCF-7 and HepG2 cells. Furthermore, we used a CLSM to visualize the mitochondrial co-localization of IR780-CSOSA on MCF-7 cells. Increased intensity of green and yellow fluorescences (merged by red and green fluorescence) was viewed with the increasing time after the treatment with IR780-CSOSA micelles (Figure 3A, 3B, 3C and and S8). Meanwhile, we found that most of IR780-CSOSA/DOX were rapidly internalized and transported into mitochondria of MCF-7 cells after 4 h (Figure S9). These results indicated that IR780-CSOSA micelles could target into mitochondria of tumor cells on account of the modification of lipophilic cation IR780. We further determined whether NIR-laser irradiation could affect the cellular internalization and mitochondrial targeting efficiency of IR780-CSOSA micelles. After NIR-laser irradiation, the green and yellow fluorescence increased in IR780-CSOSA group. However, the fluorescence intensity in CSOSA group kept almost constant before or after laser irradiation (Figure S8). The above results suggested IR780-CSOSA micelles showed improved capabilities in terms of both cellular uptake and mitochondrial targeting on MCF-7 cells upon the laser irradiation, which contributed to the increased membrane permeability and fluidity upon photothermal conversion [35, 55]. Moreover, previous study has shown that both tumor cell uptake and mitochondria trafficking of micelles were energy-dependent [56-58]. Given these well-established facts, it is not surprising that the hyperthermia exerted via laser irradiation contributed to more effective cellular internalization and enhanced mitochondrial targeting efficiency of IR780-CSOSA micelles.

NIR-triggered drug release inside mitochondria

To verify whether NIR-laser can trigger DOX release from IR780-CSOSA micelles into mitochondria, the recovery of DOX fluorescence was exploited as indicating drug release, due to the aggregation-caused quenching of DOX fluorescence after drug loaded into micelles [59, 60]. No dramatic fluorescence change was viewed in CSOSA/DOX group before or after laser irradiation, and the faint fluorescence was found to uniformly distribute in the cytoplasm (Figure 4A and S10). By comparison, IR780-CSOSA/DOX after NIR-laser irradiation exhibited noticeably enhanced DOX fluorescence, and the strong red fluorescence was mainly distributed in the mitochondria, suggesting the release of DOX into mitochondia as a consequence of hyperthermia-
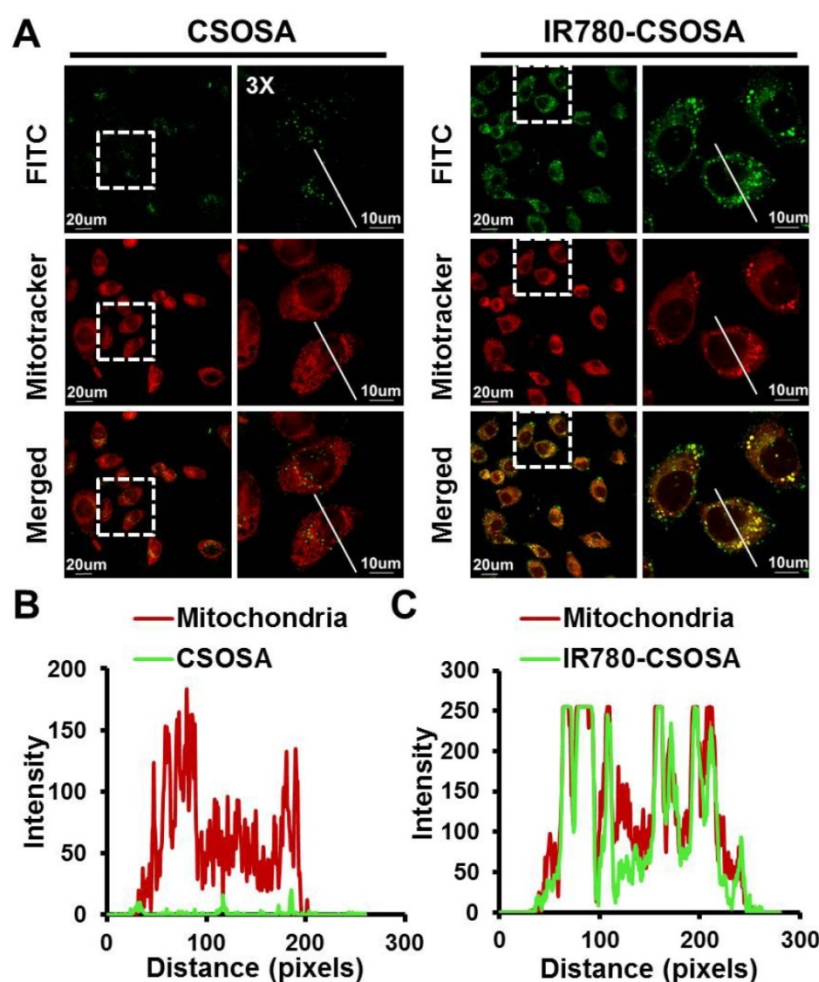
Figure 3. Cellular uptake and mitochondrial co-localization of IR780-CSOSA micelles in MCF-7 cells. (A) MCF-7 cells were incubated with FITC-labeled CSOSA or IR780-CSOSA micelles (green) for 4 h observed by CLSM. Yellow spots in the merged pictures denoted the co-localization of the micelles within mitochondrial compartments. Red: Mitotracker red. (B) The line scanning profiles of CSOSA micelles and mitochondria in the corresponding confocal images in A. (C) The line scanning profiles of IR780-CSOSA micelles and mitochondria in the corresponding confocal images in A.

induced drug release as discussed earlier (Figure 4A, 4B, 4C and S10). These results indicated that NIR-laser irradiation could effectively stimulate mitochondrial-specific drug release from IR780-CSOSA micelles to augment local DOX concentration.

In vitro chemo-photothermal therapy efficiency

The combinational therapeutic effect mediated by IR780-CSOSA/DOX under laser irradiation was tested *in vitro*. Without irradiation, the cytotoxicity of IR780-CSOSA/DOX (equivalent DOX: 3 µg/mL) micelles significantly increased in MCF-7 cells (cell viability: 51.3%), compared to that of CSOSA/DOX (59.2%) and DOX (61.1%) in the same condition (Figure 5A). This was attributed to the effective cellular internalization and mitochondrial targeting ability of IR780-CSOSA, accelerating the intracellular trafficking of DOX into mitochondria. After laser irradiation, it was found that IR780-CSOSA/DOX showed remarkable antitumor activity (cell viability:

18.3%), while the cytotoxicity induced by CSOSA/ DOX or DOX was not significantly affected after the laser irradiation. Moreover, as compared to the combination therapy mediated by IR780-CSOSA/ DOX, exclusive photothermal conversion mediated by IR780-CSOSA appeared to be much less effective, especially when the equivalent DOX concentration was 0.5 µg/mL (Figure 5B). In sharp contrast, the cell viability of IR780-CSOSA micelles against MCF-7 cells without laser irradiation was higher than 90%, which implied the low cytotoxicity nature of IR780-CSOSA micelles. Moreover, IC_{50} values of IR780-CSOSA micelles against normal fibroblast cells (NIH 3T3 cells) were above 500 µg/mL (Figure S11), indicating that IR780-CSOSA was possessed of comparatively good biocompatibility. These results implied that IR780-CSOSA/DOX can realize rapid drug release in the mitochondria after NIR-laser irradiation, which considerably enhanced mitochondrial DOX concentration to exert a better tumor inhibition effect [61]. From these results, we confirmed that the
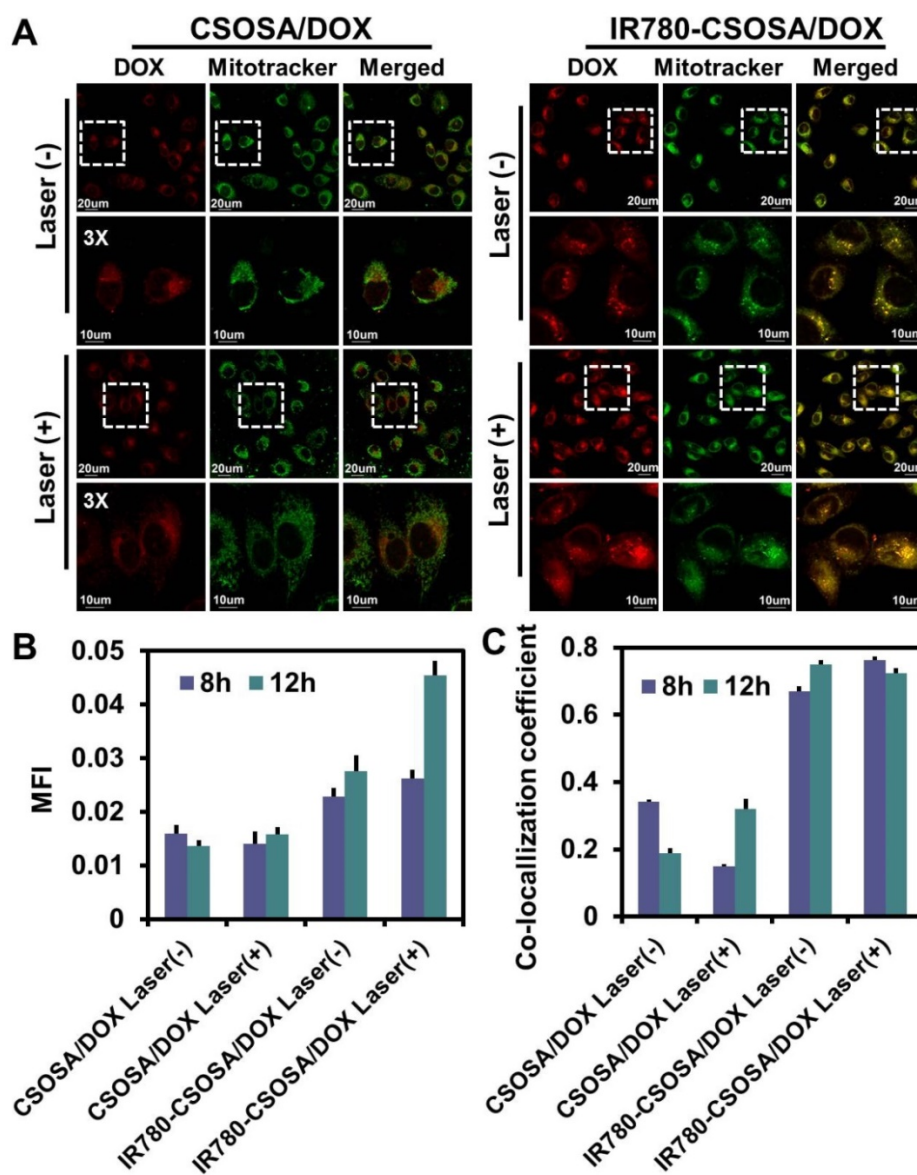
Figure 4. NIR-triggered drug release inside mitochondria in MCF-7 cells. (A) MCF-7 cells were treated with CSOSA/DOX or IR780-CSOSA/DOX (equivalent DOX: 1.5 µg/mL) for 4 h. Next, the culture medium were replaced with fresh medium to remove the uninternalized nanoparticles and irradiated with or without laser (808 nm, 1 W/cm^2) for 3 min, then continuously incubated for 4 h to observe the NIR-triggered DOX release in mitochondria by CLSM. White dotted lines denoted the corresponding magnified area. Green: Mitotracker green. Red: DOX. Yellow spots in the merged pictures denoted the co-localization of released DOX within mitochondrial compartments. (B) The mean fluorescence intensity (MFI) analysis of released DOX in the corresponding confocal images in Figure S7. (C) The co-localization coefficient of released DOX and mitochondria in the corresponding confocal images in Figure S7.

external laser stimulation could not only trigger efficient photothermal conversion, but also achieve mitochondria-specific drug targeting and release to destruct cancer cells.

Mitochondrial apoptosis signaling pathways

In order to illustrate the underlying mechanism of combinational therapeutic effect, we analyzed the expression levels of the related proteins. Firstly, HSP70, an indicator of heat stress to defend cells from oxidative or thermal stress [62], was found to be up-regulated after the treatment with IR780-CSOSA/DOX upon laser irradiation (Figure 5E). Notably, a positive correlation was found between the degree of up-regulation and the irradiation time, confirming the heat stress that the cells were subjected to [29]. Cellular ROS generation (approximately up to 90%) primarily occurred in mitochondria [56], and mitochondrial damage is closely correlated with high levels of ROS [63]. For IR780-CSOSA/DOX group, ROS levels enhanced significantly without laser irradiation, which were much higher than those of free DOX (Figure 5C and 5D). We assume that under such conditions, more DOX molecules were delivered into mitochondria, thereby inducing higher levels of ROS. Interestingly, under the laser irradiation, the generation of ROS in IR780-CSOSA group increased dramatically. The much higher levels of ROS in

laser-stimulated IR780-CSOSA group were probably due to the heat shock-mediated evolution of ROS levels [21, 22, 64]. Notably, ROS levels in IR780-CSOSA/DOX group under laser irradiation were the highest among all groups, which were 2.85 folds those of DOX or 1.93 folds those of IR780-CSOSA under the laser irradiation. These results illustrated that NIR-laser irradiation on the combined chemo-photothermal therapy could synergistically stimulate ROS evolution and elevation. On one hand, IR780-CSOSA/DOX micelles could selectively target into tumor mitochondria and realize photothermal conversion upon NIR-laser irradiation, which induced heat shock to elevate mitochondrial ROS. On the other hand, photothermally triggered internalization and DOX release, as indicated by much stronger red fluorescence inside mitochondria, could significantly enhance mitochondrial ROS generation. The high levels of ROS subsequently promote prompt mitochondria depolarization to facilitate the translocation of cytochrome c to cytosol, a process that is considered as a significant indicator of cell apoptosis [65]. As shown in Figure 5F, the content of cytochrome c in the cytosol was significantly enhanced in the IR780-CSOSA/DOX with laser group, which was greater than that in DOX or IR780-CSOSA group in the same condition. As a consequence, the translocation of cytochrome c can motivate a cascade of caspases reaction [12]. Therefore, we also observed a considerable rise in the expression of cleaved caspase-9 and cleaved caspase-3 was in the IR780-CSOSA/DOX with laser group. These results further indicated that cell apoptosis was regulated by intrinsic mitochondrial pathway. Overall, the combined chemo-photothermal therapy enhanced the evolution of high-level ROS, which efficiently activated tumor cells apoptosis. It demonstrated that both photothermally triggered DOX release and heat stress at mitochondria jointly gave rise to enhanced antitumor efficiency.
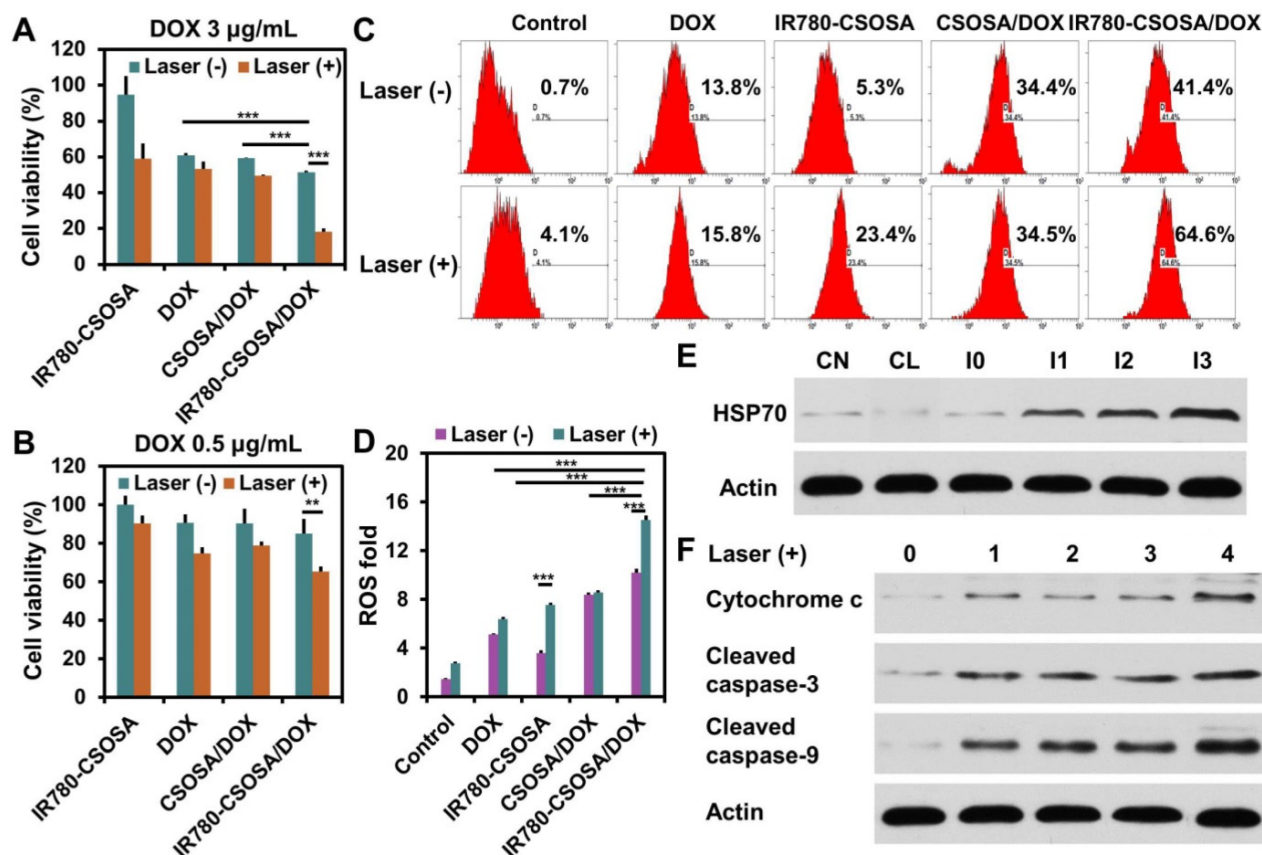

Figure 5. *In vitro* chemo-photothermal therapy efficiency. The cytotoxicity of different formulations against MCF-7 cells with or without laser irradiation at different DOX concentrations (A: equivalent DOX: 3 µg/mL, B: equivalent DOX: 0.5 /mL) for 48 h. (n = 3) (C) ROS generation in MCF-7 cells after treatment with different formulations with or without laser irradiation determined by flow cytometry. (D) Quantitative analysis on ROS levels. (E) Expression of HSP70 in MCF-7 cells was tested by western blot (CN: control without laser irradiation; CL: control with laser irradiation for 3min; I0: treatment with IR780-CSOSA/DOX without laser irradiation; I1, I2, and I3 represent treatments with IR780-CSOSA/DOX for 1, 2, and 3 min of laser irradiation, respectively. (F) Expression of apoptosis related proteins in MCF-7 cells treated with different formulations under laser irradiation. 0: control, 1: DOX, 2: CSOSA/DOX, 3: IR780-CSOSA, 4: IR780-CSOSA/DOX. Cytochrome c, cleaved caspase-3 and cleaved caspase-9 were tested by western blot. The conditions of laser irradiation are all at 808 nm with 1 W/cm² for 3 min. ***P < 0.001, **P < 0.01.
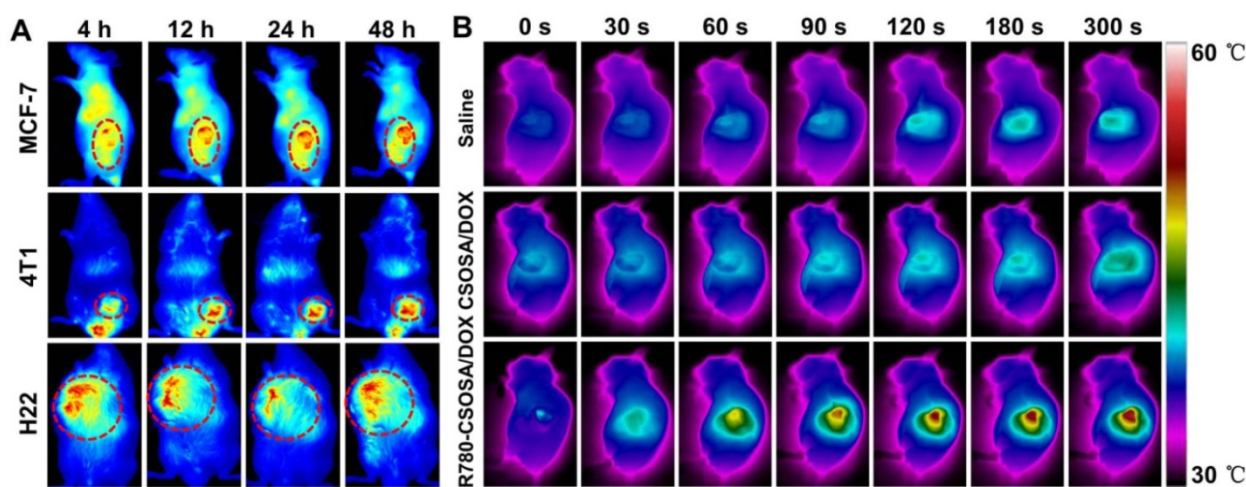
Figure 6. *In vivo* fluorescent and photothermal imaging. (A) *In vivo* NIR fluorescence imaging in MCF-7 or 4T1 or H22 tumor models of IR780-CSOSA micelles after intravenous injection for 4, 12, 24 and 48 h., respectively. (B) Infrared thermal images of MCF-7 tumor-bearing mice intravenously injected with saline, CSOSA/DOX, IR780-CSOSA/DOX during 5 min of laser irradiation (808 nm, 0.5 W/cm^2), respectively.

In vivo diagnosis and imaging

Due to the modification of IR780, an excellent probe for NIR fluorescence imaging [38, 66], IR780-CSOSA micelles may independently realize the real-time diagnosis and imaging on the tumor. To confirm this notion, we studied the tumor targeting capacity of IR780-CSOSA with three different tumor models, MCF-7 or 4T1 or H22 tumor-xenografted mice (Figure 6A). In three models, the fluorescence signal of IR780-CSOSA largely accumulated in tumor region, and the fluorescence signal enhanced in tumor with the time. Due to the high membrane potential and overexpressed organic-anion-transporting polypeptide (OATP) transporters in tumor cells, IR780-modified micelles may preferentially accumulate in tumor tissues over other tissues [43, 67, 68]. Concurrently, the IR780-modified micelles could emit NIR fluorescent signals under NIR excitation, which benefited the *in vivo* detection and tracking of IR780-CSOSA in a real-time fashion. Therefore, IR780-CSOSA micelles could be a potential probe for the diagnosis and imaging of the tumor.

Temperature measurement under NIR-laser irradiation *in vivo*

Since the elevation of temperature is significant to initiate cell death and NIR-triggered drug release in PTT [54], the temperature change of IR780-CSOSA/DOX micelles in the tumor region was measured. As shown in Figure 6B, under the laser irradiation up to 5 min, the tumor temperature of mice in IR780-CSOSA/DOX group rapidly increased to the peak 56.4 °C, which was well above the damage threshold required for irreversible tissue damage [69, 70]. In contrast, the tumor temperature in mice injected with saline or CSOSA/DOX only raised below 43 °C under the same condition, that was insufficient to induce irreversible

tumor damage [35, 71]. It indicated that IR780-CSOSA/DOX micelles are potential to be used for *in vivo* photothermal therapy.

The penetration study *in vitro* and *in vivo*

For further investigation of influence by laser-caused hyperthermia on tumor accumulation and penetration capability, we applied MCTS to evaluate the accumulation and penetration capacity of IR780-CSOSA/DOX micelles under laser irradiation (Figure 7A). IR780-CSOSA/DOX with laser group showed the best penetration profile with strong red fluorescence of DOX signal in most of areas, even at the depth of 100 μm from the periphery towards the center, demonstrating that IR780-CSOSA/DOX can commendably penetrate into deep tumor tissues under laser irradiation. In contrast, the MCTS in CSOSA/DOX with or without laser group just exhibited the DOX distribution at the periphery, with unnoticeable signal in the center of MCTS. To support our hypothesis *in vivo*, MCF-7 tumor-xenografted mice were injected intravenously with IR780-CSOSA/DOX or CSOSA/DOX micelles for one day and tumors were treated with or without laser for 3 min at 0.5 W/cm^2. After another day, the mice were euthanized and tumors were collected. The red fluorescence intensity of IR780-CSOSA/DOX micelles distributed in tumor tissues was higher than that of CSOSA/DOX, indicating that IR780-CSOSA/DOX micelles had a better accumulation capability into deep tumor tissues. After the laser irradiation, the fluorescence signal of CSOSA/DOX micelles only slightly changed, whereas the fluorescence signal of IR780-CSOSA/DOX micelles increased significantly (Figure 7B). It suggested that NIR-laser irradiation can promote the accumulation and penetration of IR780-CSOSA/DOX micelles into tumor tissues. The

deep penetration capability of IR780-CSOSA/DOX micelles under laser irradiation may arise from accelerated tumor blood flow and increased vascular pore size [72, 73], as well as enhanced cellular internalization and trafficking into mitochondria [35, 55]. Collectively, IR780-CSOSA/DOX micelles with laser were able to efficiently be accumulated in the majority of tumor regions and deliver drug cargos from the periphery to the center of solid tumor that could not only contribute to produce irreversible cell injury at the central region of the tumor, but also immensely restrain reversible cell responses and aggravate cell death at the peripheral sublethal tumor region through synergistically promoting ROS evolution activated by the photothermal-induced mitochondrial drug release as well as heat stress at tumor mitochondria.

The chemo-photothermal therapy efficiency *in vivo*

To evaluate the synergetic chemo-photothermal therapy efficacy, MCF-7 tumor-bearing mice models were injected with specified formulations with or without laser. Under laser irradiation, the tumor volume in IR780-CSOSA/DOX group decreased significantly, however, the tumor volume in other groups showed slight changes (Figure S12). With treatment proceeding, the tumor in IR780-CSOSA/DOX with laser group turned almost disappeared and the scar on the original tumor site recovered (Figure S13). Meanwhile, the tumor growth curve after administration showed that IR780-CSOSA/DOX with equivalent dose after laser irradiation was the most effective in inhibiting tumor growth (tumor inhibition rate: 85.3%), compared with DOX·HCl group (55.0%) and photothermal IR780-CSOSA group (54.7%)
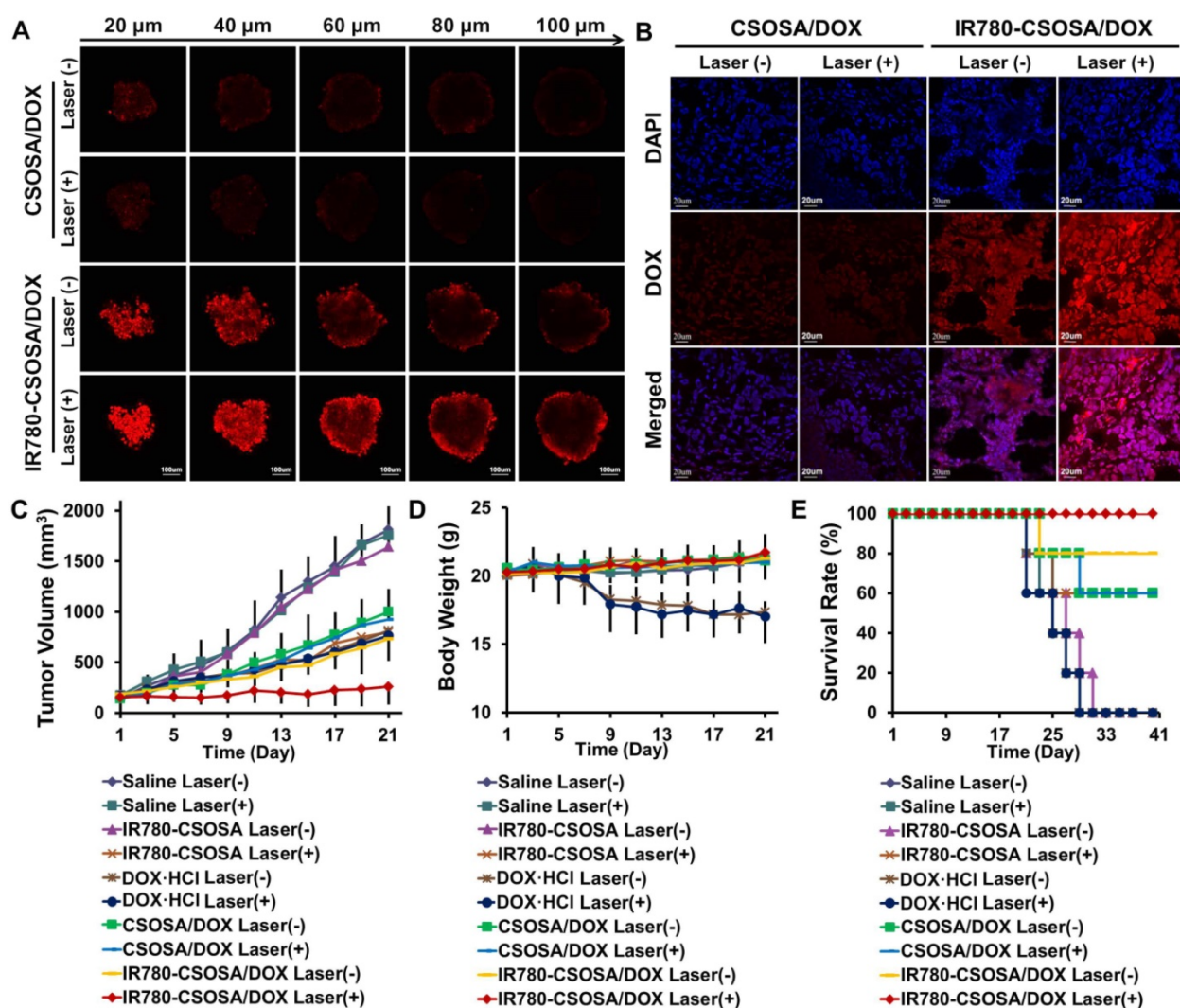

Figure 7. The evaluation on chemo-photothermal therapy of IR780-CSOSA/DOX micelles *in vivo*. (A) *In vitro* penetration of CSOSA/DOX and IR780-CSOSA/DOX micelles into the MCTS irradiated with or without laser (808 nm, 1 W/cm², 3 min). Z-stack images using CLSM were obtained from the top to the equatorial plane of MCTS. Scale bar: 100 μm. (B) *In vivo* penetration of micelles into the tumors of MCF-7 tumor-bearing nude mice. The frozen tumor sections were observed using CLSM. Scale bar: 20 μm. (C) Tumor volumes of MCF-7 tumor-xenografted mice in different groups with or without laser irradiation (808 nm, 0.5 W/cm², 3 min) (equivalent DOX dosage: 2 mg/kg). (mean ± SD, n = 6). (D) Body weight variation. (mean ± SD, n = 6). (E) Survival rates.

(Figure 7C). Obviously, a severe weight loss in DOX·HCl group with or without laser irradiation was found (Figure 7D), indicating severe systemic side effects. However, IR780-CSOSA/DOX with or without laser irradiation group displayed a similar slight increase in body weight as the saline-treated group. These results implied that IR780-CSOSA/DOX and NIR-laser irradiation generated very low systemic toxicity. Immunohistological analysis indicated that the slices of major organs (Figure S14 and S15) from DOX·HCl with or without laser irradiation group showed clear cardiac damage in the heart section and pathological changes as well as necrosis in the liver section, while those from micelle-treated groups exhibited unnoticeable pathological changes in comparison with those from saline-treated group, proving the negligible organ damage and low toxicity nature of micelles. Survival time of these mice was recorded after treatment (Figure 7E). The chemo-photothermal IR780-CSOSA/DOX group showed the longest median survival time with 100% survival rate and there was no tumor recurrence during a therapeutic window of 40 days. In contrast, only 60% of mice could survive in the photothermal IR780-CSOSA group after the treatment, and none of mice survived in DOX·HCl group. HE images (Figure S16) showed that most of tumor cells after the treatment by IR780-CSOSA/DOX formulation under the laser irradiation became severely apoptotic and necrotic. These results indicated that the chemo-photothermal IR780-CSOSA/DOX micelles exhibited a great advantage with outstanding antitumor efficiency and lower systemic toxicity.

In order to explore the underlying reason of the high antitumor efficiency of combined chemo-photothermal IR780-CSOSA/DOX micelles *in vivo*, we performed the immunohistochemistry analysis on tumor tissues in all the groups. Firstly, tumor tissues were stained with HSP70 antibody to further investigate the heat stress of cells *in vivo*. HSP70 expression in tumors of IR780-CSOSA/DOX group increased remarkably after laser irradiation, suggesting the local hyperthermia in tumor tissues (Figure 8A and 8B). However, there was no distinction in HSP70 expression between control groups with or without laser irradiation. The expression of cleaved caspase-3 (brown) in tumors of IR780-CSOSA/DOX group under laser irradiation increased sharply, suggesting the significant apoptosis (Figure 8C, 8D, S17 and S18). The percentage of Ki67-positive cells (brown) in tumors from the combinational chemo-phototherapy group was the lowest among all groups. We also further verified whether combined chemo-photothermal

therapy induced the inhibition of blood vessels and activation of host immune response (Figure 8C, 8D, S17 and S18). Surprisingly, IR780-CSOSA/DOX with laser irradiation restrained the angiogenesis of blood vessel by decreasing the levels of CD 31 (brown) and activated the host immune response with enhanced recruit of CD 8^{+} T cells into tumor tissues (Figure 8C, 8D, S17 and S18).

Conclusions

In conclusion, a photothermal stimulation strategy was developed for mitochondria-responsive drug release along with heat shock for precise and enhanced chemo-photothermal combination therapy in the current study. The delivery carrier IR780-CSOSA could selectively accumulate in tumor cell mitochondria to exert its role of photothermal conversion, contributing to the fast DOX release inside mitochondria to product more ROS. Concurrently, photothermal conversion also induced mitochondrial heat shock, stimulating further amplification of ROS. Owing to the amplified ROS evolution, the highly accumulated DOX together with heat shock in the tumor mitochondria jointly gave rise to superadditive antitumor effects, which initiated a cascade of caspase reactions to promote tumor cell apoptosis through mitochondrial signal pathway. Furthermore, IR780-CSOSA micelles may independently realize the real-time diagnosis and imaging on multiple tumor models. Importantly, the elevated accumulation and deep penetration in tumor tissues by IR780-CSOSA/DOX could be manipulated by laser irradiation. By taking advantage of photothermal conversion ability of IR780-CSOSA, the tumor local hyperthermia was caused by the laser irradiation, which produced irreversible cell injury not only at the central region of the tumor, but also at the peripheral region that was usually difficult to cover in the photothermal therapy. The photothermal-induced mitochondrial drug release as well as heat stress at tumor mitochondria can synergistically promote ROS evolution, thereby considerably accelerating cell apoptosis at peripheral sublethal region. Collectively, our study opens up a new avenue for the future cancer diagnosis and treatment.

Supplementary Material

Supplementary figures and tables.
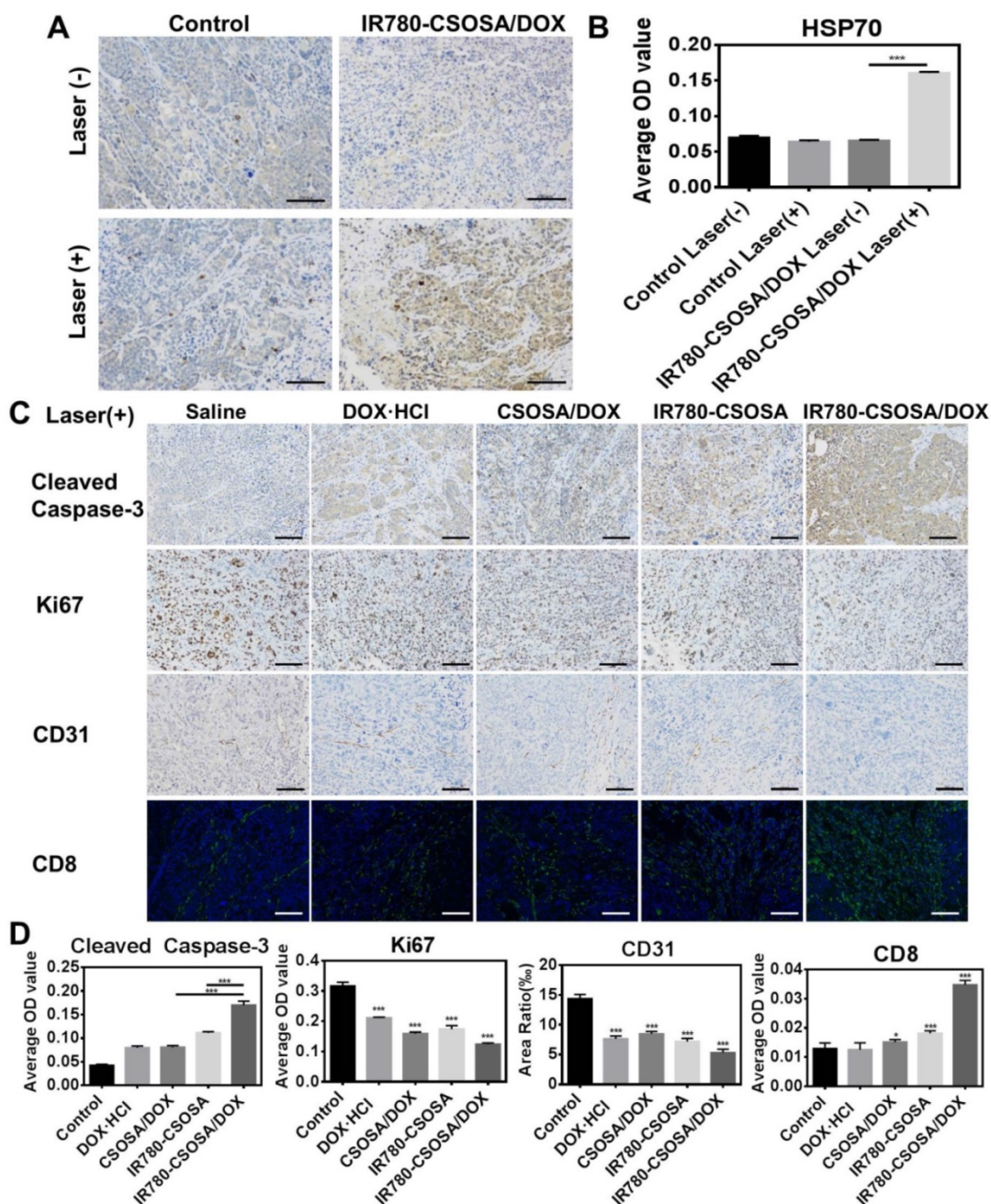http://www.thno.org/v09p0691s1.pdf

Figure 8. *In vivo* immunohistochemical analysis in MCF-7 xenograft tumors treated with IR780–CSOSA/DOX micelles-mediated chemo-photothermal therapy. (A) HSP70 protein expression (brown) in saline and IR780-CSOSA/DOX with or without laser groups. Scale bar: 100 μm. (B) The average OD value of HSP70 levels. (n = 3). (C) Under laser irradiation, the induction of apoptosis by staining with cleaved caspase-3 antibody (brown). Cell proliferation evaluation by Ki67 staining (brown). Tumor blood vessel staining with CD 31 antibody (brown). CD 8^{+} T cells detected by immunofluorescent staining (green). Scale bar: 100 μm. (D) Under laser irradiation, the quantitative analysis of cleaved caspase-3, Ki67, CD31 and CD8 levels. (n = 3). The conditions of laser irradiation are all at 808 nm with 0.5 W/cm^2 for 3 min. ***$P < 0.001$, *$P < 0.05$

Competing Interests

The authors have declared that no competing interest exists.

References

1. Tiwari M. Nano cancer therapy strategies. J Cancer Res Ther. 2012; 8: 19-22.
2. Torchilin VP. Recent approaches to intracellular delivery of drugs and DNA and organelle targeting. Annu Rev Biomed Eng. 2006; 8: 343-75.
3. Maity AR, Stepensky D. Delivery of drugs to intracellular organelles using drug delivery systems: Analysis of research trends and targeting efficiencies. Int J Pharm. 2015; 496: 268-74.
4. Wallace DC. Mitochondrial diseases in man and mouse. Science. 1999; 283: 1482-8.
5. Wallace DC. Mitochondria and cancer. Nat Rev Cancer. 2012; 12: 685-98.
6. Zhang D, Wen L, Huang R, Wang H, Hu X, Xing D. Mitochondrial specific photodynamic therapy by rare-earth nanoparticles mediated near-infrared graphene quantum dots. Biomaterials. 2018; 153: 14-26.
7. Modicanapolitano JS, Aprille JR. Delocalized lipophilic cations selectively target the mitochondria of carcinoma cells. Adv Drug Deliv Rev. 2001; 49: 63-70.
8. Sean Marrache SD. Engineering of blended nanoparticle platform for delivery of mitochondria-acting therapeutics. P Natl Acad Sci U S A. 2012; 109: 16288-93.
9. HH S. Mitochondria-targeted peptide antioxidants: Novel neuroprotective agents. Aaps Journal. 2006; 8: E521-E31.
10. HH S. Cell-permeable, mitochondrial-targeted, peptide antioxidants. Aaps Journal. 2006; 8: E277-E83.

11. Xiong H, Du S, Ni J, Zhou J, Yao J. Mitochondria and nuclei dual-targeted heterogeneous hydroxyapatite nanoparticles for enhancing therapeutic efficacy of doxorubicin. Biomaterials. 2016; 94: 70-83.

12. Zhou J, Zhao WY, Ma X, Ju RJ, Li XY, Li N, et al. The anticancer efficacy of paclitaxel liposomes modified with mitochondrial targeting conjugate in resistant lung cancer. Biomaterials. 2013; 34: 3626-38.

13. Sarandeep Singh M, Murthy RSR. Delivery to mitochondria: a narrower approach for broader therapeutics. Expert Opin Drug Del. 2012; 9: 909-35.

14. Nanowerk S, Nano L. Nanocarriers boost cancer drug efficacy by targeting specific sites inside tumor cells. Nano Lett. 2008.

15. Wen R, Banik B, Pathak RK, Kumar A, Kolishetti N, Dhar S. Nanotechnology inspired tools for mitochondrial dysfunction related diseases. Adv Drug Deliv Rev. 2016; 99: 52-69.

16. Zielonka J, Joseph J, Sikora A, Hardy M, Ouari O, Vasquez-Vivar J, et al. Mitochondria-Targeted Triphenylphosphonium-Based Compounds: Syntheses, Mechanisms of Action, and Therapeutic and Diagnostic Applications. Chem Rev. 2017; 117: 10043-120.

17. Biswas S, Torchilin VP. Nanopreparations for organelle-specific delivery in cancer. Adv Drug Deliv Rev. 2014; 66: 26-41.

18. Wong PT, Choi SK. Mechanisms of Drug Release in Nanotherapeutic Delivery Systems. Chem Rev. 2015; 115: 3388-432.

19. Green RM, Graham M, O'Donovan MR, Chipman JK, Hodges NJ. Subcellular compartmentalization of glutathione: correlations with parameters of oxidative stress related to genotoxicity. Mutagenesis. 2006; 21: 383-90.

20. Guzy RD, Schumacker PT. Oxygen sensing by mitochondria at complex III: the paradox of increased reactive oxygen species during hypoxia. Exp Physiol. 2006; 91: 807-19.

21. Willis WT, Jackman MR, Bizeau ME, Pagliassotti MJ, Hazel JR. Hyperthermia impairs liver mitochondrial function in vitro. Am J Physiol Regul Integr Comp Physiol. 2000; 278: R1240-6.

22. Flanagan SW, Moseley PL, Buettner GR. Increased flux of free radicals in cells subjected to hyperthermia: detection by electron paramagnetic resonance spin trapping. FEBS Lett. 1998; 431: 285-6.

23. L Z, FL C, VP W, CY L, AJ M, LJ B, et al. Intra- and extracellular measurement of reactive oxygen species produced during heat stress in diaphragm muscle. Am J Physiol Cell Physiol. 2000; 279: 1058-66.

24. Pan GY, Jia HR, Zhu YX, Wu FG. Turning double hydrophilic into amphiphilic: IR825-conjugated polymeric nanomicelles for near-infrared fluorescence imaging-guided photothermal cancer therapy. Nanoscale. 2018; 10: 2115-27.

25. Pan GY, Jia HR, Zhu YX, Sun W, Cheng XT, Wu FG. Cyanine-Containing Polymeric Nanoparticles with Imaging/Therapy-Switchable Capability for Mitochondria-Targeted Cancer Theranostics. ACS Appl Nano Mater. 2018; 1: 2885-97.

26. Pan GY, Jia HR, Zhu YX, Wang RH, Wu FG, Chen Z. Dual Channel Activatable Cyanine Dye for Mitochondrial Imaging and Mitochondria-Targeted Cancer Theranostics. ACS Biomater Sci Eng. 2017; 3: 3596-606.

27. Jung HS, Han J, Lee JH, Ji HL, Choi JM, Kweon HS, et al. Enhanced NIR Radiation-Triggered Hyperthermia by Mitochondrial Targeting. J Am Chem Soc. 2015; 137: 3017-23.

28. Shah BP, Pasquale N, De G, Tan T, Ma J, Lee KB. Core-Shell Nanoparticle-Based Peptide Therapeutics and Combined Hyperthermia for Enhanced Cancer Cell Apoptosis. ACS Nano. 2014; 8: 9379-87.

29. Luo S, Tan X, Fang S, Wang Y, Liu T, Wang X, et al. Mitochondria-Targeted Small-Molecule Fluorophores for Dual Modal Cancer Phototherapy. Adv Funct Mater. 2016; 26: 2826-35.

30. Yu Z, Sun Q, Pan W, Li N, Tang B. A Near-Infrared Triggered Nanophotosensitizer Inducing Domino Effect on Mitochondrial Reactive Oxygen Species Burst for Cancer Therapy. ACS Nano. 2015; 9: 11064-74.

31. Fei Y, Duan W, Li Y, Hao W, Zhou Y, Min P, et al. NIR-Laser-Controlled Drug Release from DOX/IR-780-Loaded Temperature-Sensitive-Liposomes for Chemo-Photothermal Synergistic Tumor Therapy. Theranostics. 2016; 6: 2337-51.

32. Liao JF, Li WT, Peng JR, Yang Q, Li H, Wei YQ, et al. Combined Cancer Photothermal-Chemotherapy Based on Doxorubicin/Gold Nanorod-Loaded Polymersomes. Theranostics. 2015; 5: 345-56.

33. Wang C, Xu L, Liang C, Xiang J, Peng R, Liu Z. Immunological Responses Triggered by Photothermal Therapy with Carbon Nanotubes in Combination with Anti-CTLA-4 Therapy to Inhibit Cancer Metastasis. Adv Mater. 2014; 26: 8154-62.

34. Zhang Z, Wang J, Chen C. Near-infrared light-mediated nanoplatforms for cancer thermo-chemotherapy and optical imaging. Adv Mater. 2013; 25: 3869-80.

35. Zheng M, Yue C, Ma Y, Gong P, Zhao P, Zheng C, et al. Single-step assembly of DOX/ICG loaded lipid-polymer nanoparticles for highly effective chemo-photothermal combination therapy. ACS Nano. 2013; 7: 2056-67.

36. Zheng T, Li GG, Zhou F, Wu R, Zhu JJ, Wang H. Gold-Nanosponge-Based Multistimuli-Responsive Drug Vehicles for Targeted Chemo-Photothermal Therapy. Adv Mater. 2016; 28: 8218-26.

37. Zubareva AA, Shcherbinina TS, Varlamov VP, Svirshchevskaya EV. Intracellular sorting of differently charged chitosan derivatives and chitosan-based nanoparticles. Nanoscale. 2015; 7: 7942-52.

38. Peng CL, Shih YH, Lee PC, Hsieh TM, Luo TY, Shieh MJ. Multimodal image-guided photothermal therapy mediated by 188Re-labeled micelles containing a cyanine-type photosensitizer. ACS Nano. 2011; 5: 5594-607.

39. Luo S, Tan X, Fang S, Wang Y, Liu T, Wang X, et al. Cancer Phototherapy: Mitochondria-Targeted Small-Molecule Fluorophores for Dual Modal Cancer Phototherapy (Adv. Funct. Mater. 17/2016). Adv Funct Mater. 2016; 26: 2975.

40. Tan X, Luo S, Long L, Wang Y, Wang D, Fang S, et al. Structure-Guided Design and Synthesis of a Mitochondria-Targeting Near-Infrared Fluorophore with Multimodal Therapeutic Activities. Adv Mater. 2017; 29: 1704196.

41. Wang Y, Liu T, Zhang E, Luo S, Tan X, Shi C. Preferential accumulation of the near infrared heptamethine dye IR-780 in the mitochondria of drug-resistant lung cancer cells. Biomaterials. 2014; 35: 4116-24.

42. Yuan A, Qiu X, Tang X, Liu W, Wu J, Hu Y. Self-assembled PEG-IR-780-C13 micelle as a targeting, safe and highly-effective photothermal agent for in vivo imaging and cancer therapy. Biomaterials. 2015; 51: 184-93.

43. Zhang C, Liu T, Su Y, Luo S, Zhu Y, Tan X, et al. A near-infrared fluorescent heptamethine indocyanine dye with preferential tumor accumulation for in vivo imaging. Biomaterials. 2010; 31: 6612-7.

44. Tan Y, Zhu Y, Zhao Y, Wen L, Meng T, Liu X, et al. Mitochondrial alkaline pH-responsive drug release mediated by Celastrol loaded glycolipid-like micelles for cancer therapy. Biomaterials. 2018; 154: 169-81.

45. Hu YW, Du YZ, Liu N, Liu X, Meng TT, Cheng BL, et al. Selective redox-responsive drug release in tumor cells mediated by chitosan based glycolipid-like nanocarrier. J Control Release. 2015; 206: 91-100.

46. Liu SQ, Wiradharma N, Gao SJ, Tong YW, Yang YY. Bio-functional micelles self-assembled from a folate-conjugated block copolymer for targeted intracellular delivery of anticancer drugs. Biomaterials. 2007; 28: 1423-33.

47. Liu N, Tan Y, Hu Y, Meng T, Wen L, Liu J, et al. A54 Peptide Modified and Redox-Responsive Glucolipid Conjugate Micelles for Intracellular Delivery of Doxorubicin in Hepatocarcinoma Therapy. ACS Appl Mater Interfaces. 2016; 8: 33148-56.

48. Li S, Girod-Holland S, Vert M. Hydrolytic degradation of poly(dl -lactic acid) in the presence of caffeine base. J Control Release. 1996; 40: 41-53.

49. Tan Y, Zhu Y, Zhao Y, Wen L, Meng T, Liu X, et al. Mitochondrial alkaline pH-responsive drug release mediated by Celastrol loaded glycolipid-like micelles for cancer therapy. Biomaterials. 2018; 154: 169-81.

50. Miyajima M, Koshika A, Okada J, Ikeda M. Effect of polymer/basic drug interactions on the two-stage diffusion-controlled release from a poly(L-lactic acid) matrix. J Control Release. 1999; 61: 295-304.

51. Miyajima M, Koshika A, Okada JI, Ikeda M. Mechanism of drug release from poly(l -lactic acid) matrix containing acidic or neutral drugs. J Control Release. 1999; 60: 199-209.

52. Miyajima M, Koshika A, Okada JI, Kusai A, Ikeda M. The effects of drug physico-chemical properties on release from copoly (lactic/glycolic acid) matrix. Int J Pharm. 1998; 169: 255-63.

53. Guo X, Li D, Yang G, Shi C, Tang Z, Wang J, et al. Thermo-triggered drug release from actively targeting polymer micelles. ACS Appl Mater Interfaces. 2014; 6: 8549-59.

54. Su J, Sun H, Meng Q, Yin Q, Zhang P, Zhang Z, et al. Bioinspired Nanoparticles with NIR-Controlled Drug Release for Synergetic Chemophotothermal Therapy of Metastatic Breast Cancer. Adv Funct Mater. 2016; 26: 7495-506.

55. Tang Y, Lei T, Manchanda R, Nagesetti A, Fernandezfernandez A, Srinivasan S, et al. Simultaneous delivery of chemotherapeutic and thermal-optical agents to cancer cells by a polymeric (PLGA) nanocarrier: an in vitro study. Pharm Res. 2010; 27: 2242-53.

56. Hoye AT, Davoren JE, Wipf P, Fink MP, Kagan VE. Targeting mitochondria. Acc Chem Res. 2008; 41: 87-97.

57. Kam NWS, Liu Z, Dai H. Carbon Nanotubes as Intracellular Transporters for Proteins and DNA: An Investigation of the Uptake Mechanism and Pathway. Angew Chem. 2006; 118: 591-5.

58. Sherlock SP, Tabakman SM, Xie L, Dai H. Photothermally Enhanced Drug Delivery by Ultra-Small Multifunctional FeCo/Graphitic-Shell Nanocrystals. ACS Nano. 2011; 5: 1505-12.

59. Liow SS, Dou Q, Kai D, Li Z, Sugiarto S, Yu CY, et al. Long-Term Real-Time In Vivo Drug Release Monitoring with AIE Thermogelling Polymer. Small. 2017; 13: 1603404.

60. Liu J, Wang C, Wang X, Wang X, Cheng L, Li Y, et al. Mesoporous Silica Coated Single-Walled Carbon Nanotubes as a Multifunctional Light-Responsive Platform for Cancer Combination Therapy. Adv Funct Mater. 2015; 25: 384-92.

61. Bogart LK, Taylor A, Cesbron Y, Murray P, Lévy R. Photothermal microscopy of the core of dextran-coated iron oxide nanoparticles during cell uptake. ACS Nano. 2012; 6: 5961-71.

62. Chen H, Adam A, Cheng Y, Tang S, Hartung J, Bao E. Localization and expression of heat shock protein 70 with rat myocardial cell damage induced by heat stress in vitro and in vivo. Mol Med Report. 2015; 11: 2276-84.

63. Guido K, Lorenzo G, Catherine B. Mitochondrial Membrane Permeabilization in Cell Death. Physiol Rev. 2007; 87: 99-163.

64. Zuo L, Christofi FL, Wright VP, Liu CY, Merola AJ, Berliner LJ, Clanton TL. Intra- and extracellular measurement of reactive oxygen species produced during heat stress in diaphragm muscle. Am J Physiol Cell Physiol. 2000; 279: C1058-C66.

65. Lee JH, Won YS, Park KH, Lee MK, Tachibana H, Yamada K, et al. Celastrol inhibits growth and induces apoptotic cell death in melanoma cells via the

activation ROS-dependent mitochondrial pathway and the suppression of PI3K/AKT signaling. Apoptosis. 2012; 17: 1275-86.

66. Chen Y, Li Z, Wang H, Wang Y, Han H, Jin Q, et al. IR-780 Loaded Phospholipid Mimicking Homopolymeric Micelles for Near-IR Imaging and Photothermal Therapy of Pancreatic Cancer. ACS Appl Mater Interfaces. 2016; 8: 6852-8.

67. Erlong Z, Shenglin L, Xu T, Chunmeng S. Mechanistic study of IR-780 dye as a potential tumor targeting and drug delivery agent. Biomaterials. 2014; 35: 771-8.

68. Wang Y, Liu T, Zhang E, Luo S, Tan X, Shi C. Preferential accumulation of the near infrared heptamethine dye IR-780 in the mitochondria of drug-resistant lung cancer cells. Biomaterials. 2014; 35: 4116-24.

69. Mou J, Lin T, Huang F, Shi J, Chen H. A New Green Titania with Enhanced NIR Absorption for Mitochondria-Targeted Cancer Therapy. Theranostics. 2017; 7: 1531-42.

70. Peng CL, Shih YH, Lee PC, Hsieh MH, Luo TY, Shieh MJ. Multimodal Image-Guided Photothermal Therapy Mediated by 188Re-Labeled Micelles Containing a Cyanine-Type Photosensitizer. ACS Nano. 2011; 5: 5594-607.

71. Zhang J, Jin W, Wang X, Wang J, Zhang X, Zhang Q. A novel octreotide modified lipid vesicle improved the anticancer efficacy of doxorubicin in somatostatin receptor 2 positive tumor models. Mol Pharm. 2010; 7: 1159-68.

72. Gormley AJ, Larson N, Sadekar S, Robinson R, Ray A, Ghandehari H. Guided Delivery of Polymer Therapeutics Using Plasmonic Photothermal Therapy. Nano Today. 2012; 7: 158-67.

73. Kong G, Braun RD, Dewhirst MW. Characterization of the Effect of Hyperthermia on Nanoparticle Extravasation from Tumor Vasculature. Cancer Res. 2001; 61: 3027-32.